



10th International Conference on Applied Energy (ICAE2018), 22-25 August 2018, Hong Kong, China

Dynamic modeling of a NG-fueled SOFC-PEMFC hybrid system coupled with TSA process for fuel cell vehicle

Zhen Wu^{a,b,*}, Meng Ni^a, Pengfei Zhu^b, Zaoxiao Zhang^b

^aBuilding Energy Research Group, Department of Building and Real Estate, The Hong Kong Polytechnic University, Hong Kong, P.R.China

^bState Key Laboratory of Multiphase Flow in Power Engineering, School of Chemical Engineering and Technology, Xi'an Jiaotong University, Xi'an 710049, P.R. China

Abstract

Fuel cell power technology has drawn extensive attentions due to its high efficiency, low emission and noise. Solid oxide fuel cell (SOFC) could generate the power by diverse fuels, such as natural gas (NG), while proton exchange membrane fuel cell (PEMFC) only feeds on pure H₂. More and more attentions are paid on the combination of SOFC and PEMFC for high efficiency and convenient refueling in the practical applications. To obtain H₂ fuel with high purity from SOFC as a reformer, the gas processing subsystem for H₂ separation and purification should be applied between SOFC and PEMFC. In this present study, the gas processing subsystem, consisting of water gas shift (WGS) and thermal swing adsorption (TSA), is introduced into the SOFC-PEMFC hybrid system. Then, the SOFC-WGS-TSA-PEMFC hybrid system is modelled to investigate the transient behaviors under different operations. The simulation results show that the SOFC-WGS-TSA-PEMFC hybrid system has an improved energy conversion efficiency of approximately 64%, which is higher than the only-SOFC and the reform-PEMFC. The waste heat recovery for driving the TSA reaction accounts for the higher net electricity efficiency compared with the SOFC-PEMFC hybrid system based on the pressure swing adsorption (PSA) for H₂ separation. Since the SOFC and PEMFC have completely different transient responses to the change of the loading, the influences of operating conditions of fuel cell vehicles on the transient behaviors of single SOFC and PEMFC and the overall performance of the SOFC-WGS-TSA-PEMFC hybrid system are further investigated. Through the analysis and discussion based on the dynamic modelling, the operation strategy is unveiled in this paper for the performance optimization of the hybrid system when installed in the fuel cell vehicles.

© 2019 The Authors. Published by Elsevier Ltd.

This is an open access article under the CC BY-NC-ND license (<http://creativecommons.org/licenses/by-nc-nd/4.0/>)

Peer-review under responsibility of the scientific committee of ICAE2018 – The 10th International Conference on Applied Energy.

Keywords: SOFC; PEMFC; Metal hydride; Transient behavior; High efficiency

* Corresponding author. Tel:+852-3400-8178.

E-mail address: wuz2015@mail.xjtu.edu.cn

Nomenclature

A	active cell area, m ²
C_a	rate constant, s ⁻¹
c_p	specific heat, J/(kg K)
D_{A-B}	gas diffusion coefficient between the gas of A and B, m ² /s
D^{eff}	effective diffusion coefficient, m ² /s
D_K	Knudsen diffusion coefficient, m ² /s
E_{act}	activation energy, J/mol
E_N	reversible cell voltage, V
F	Faraday constant, 96485.338 C/mol
H/M	atomic ratio of hydrogen to metal
I	current, A
J	current density, A/m ²
J_0	exchange current density, A/m ²
J_{max}	maximum current density, A/m ²
K	reaction equilibrium constant
l	thickness, m
\dot{m}	reaction rate, kg/s
N	number of cell
P	power, kW
p	pressure, bar
R_{ohm}	Ohmic resistance, Ω
T	temperature, K
μ_{fuel}	fuel utilization
ρ	density, kg/m ³
Subscript	
a	anode
c	cathode
e	electrode
eq	equilibrium
f	fluid
in	inlet
ref	reference

1. Introduction

An efficient and clean energy utilization technology is essential for the sustainable development of society. Fuel cell power technology has drawn extensive attentions due to its high efficiency, low emission and noise [1,2]. Proton exchange membrane fuel cell (PEMFC) and solid oxide fuel cell (SOFC) are the two important kinds of fuel cells for power generation, which work at different operating conditions and thus present different electrochemical performances. The PEMFC has relatively low operating temperatures (no more than 373 K), mature fabrication technology and fast transient response [3], while the SOFC has to work at an elevated operating temperature up to more than 873 K. It is exactly because of the high operating temperature that the SOFC could operate to generate power by feeding on diverse fuels, such as CH₄, biogas, natural gas (NG) and petroleum gas through reforming and water gas shift (WGS) reactions. The fuel diversification makes the SOFC more convenient and widely applicable in the practical applications, compared with the PEMFC which can only depend on pure H₂ as fuel. Compared with H₂ fuel, NG is much cheaper and more available due to the well-developed NG refueling stations. However, poor transient behavior exists in the NG fueled SOFC due to the high operating temperature. The slow transient response of the SOFC limits its application only to stationary.

In view of the fast transient response of PEMFC and H₂ generation from SOFC by reforming CH₄, the hybrid system consisting of PEMFC and SOFC is proposed to cover the merits of both SOFC and PEMFC. The combination of SOFC and PEMFC makes the mobile application of SOFC possible and feasible. Therefore, more and more attentions have been drawn to the SOFC-PEMFC hybrid system in the mobile energy utilization systems, such as the on-board power system. Dicks et al. [4] used the SOFC as a reformer for H₂ generation and delivered H₂ to the PEMFC for more power generation. Through comparison with standalone SOFC or reformer-PEMFC power systems, it was found that SOFC-PEMFC hybrid system presents a higher overall efficiency. The net electricity efficiency could be improved by approximately 8%~16% reported by Rabbani et al. [5]. In the hybrid system, a gas processing (GP) procedure should be coupled between the SOFC and the PEMFC for H₂ separation and purification to ensure pure H₂ for the PEMFC. Otherwise, the impurity gas easily poisons the PEMFC catalyst, thus resulting in the PEMFC performance degradation, especially CO. About 10 ppm of CO can deactivate the PEMFC anodic Pt-based catalyst [6]. In order to improve the purity of H₂, Fernandes et al. [7] adopted the method of pressure swing adsorption (PSA) for H₂ separation to connect the reforming output and the PEMFC anode input in the hybrid system. Based on SOFC as a reformer to convert NG into H₂ for PEMFC, the authors proposed the innovative CaPP (Car as Power Plant) concept that the H₂ fuel from the SOFC reformer (SOFCR) is delivered into the PEMFC-powered car as the power plant to generate electricity when the car is in the parking situation. In the reported hybrid systems, pressure swing adsorption (PSA) technology is commonly applied because of its simple operation and low cost. However, it is hard to achieve high purity H₂ separation from the reformed gas mixture (H₂, CO, CO₂ and H₂O) by PSA due to that the separation is a completely physical process. The H₂ purity processed by PSA is reported to be about 96% [8]. In contrast with the PSA, the method of thermal swing adsorption (TSA) for H₂ separation and purification could achieve the purity of H₂ fuel as high as 99.9999% by chemisorption [9]. Our previous study [10] shows Al-doped AB₃-type hydrogen storage alloy (HSA) is capable of separating and purifying H₂ from the gas mixture containing CO. Consequently, the TSA incorporation between the SOFC and the PEMFC contributes to preventing the PEMFC from the poisoning of CO. Besides, the H₂ desorption temperature of AB₃-type HAS matches well with the operating temperature of PEMFC, both of which are in the range of 323 ~ 363 K. It means that the discharged H₂ can be directly feed into the PEMFC without pre-cooling or pre-heating. Also, the heat requirement for the TSA process can be derived from waste heat recovery in the SOFC-PEMFC hybrid system for improving the heat efficiency.

In the present study, the NG-fueled SOFC-PEMFC hybrid system coupled with the TSA gas processing procedure is modeled. The transient behaviors under different loading operations are investigated on the basis of the dynamic model of the hybrid system. The influences of operation strategy on the transient responses of single SOFC and PEMFC as well as the overall performances of the hybrid system are further discussed for the optimal operation strategy when the hybrid system is applied to power the fuel cell vehicles.

2. System modeling

2.1. System description

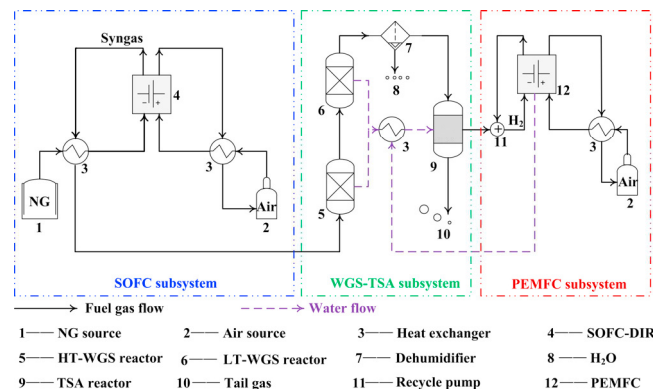


Fig. 1. Schematic diagram of the SOFC-PEMFC hybrid system coupled with TSA for H₂ separation and purification

The NG-fueled SOFC-PEMFC hybrid system coupled with the TSA consists of three main subsystems which are SOFC, GP and PEMFC, as shown in Fig. 1. The SOFC subsystem consumes the preheated NG fuel and air to produce H_2 by the reforming reaction and generate power in the meanwhile. The produced syngas mixture of CO, CO_2 , H_2 , H_2O and N_2 out of the SOFC anode will be input into the GP subsystem. In the GP subsystem, two stages of the high-temperature (HT) and low-temperature (LT) WGS reactions are first adopted for the WGS reaction of the syngas to ensure both the high converting rate (HT-WGS stage) and the large H_2 production (LT-WGS stage). Then, the treated syngas after the WGS is dried, cooled and input into the TSA reactor filled with Al-doped AB_5 -type HAS $LaNi_{4.3}Al_{0.7}$. The HAS selectively reacts with H_2 component of the syngas to form metal hydride (MH) at room temperature. Meanwhile, the other components of the syngas are exhausted to environment. When the temperature of the TSA reactor is elevated to about 323~363 K, the pure H_2 adsorbed in MH can be discharged into the PEMFC subsystem for power generation. The heat required for hydrogen desorption reaction comes from the WGS reaction heat recovery to improve the heat efficiency.

2.2. System model

The following assumptions are made in the model development.

- 1) Pressure drops in the hybrid system are neglected.
- 2) The NG source is desulfurized and CH_4 is the only hydrocarbon component. The conversion of CH_4 in H_2 is assumed to be complete in the SOFC as a reformer. The necessary heat required for the reforming reaction is taken from the electrochemical reaction of the SOFC. Besides, high steam to carbon ratio is assumed to avoid carbon deposition occurring in the SOFC [11].
- 3) In the SOFC, the CH_4 reforming reaction and electrochemical reaction are separately modeled. The gas product after the reforming reaction is the input fuel of the subsequent electrochemical reaction. Both the reforming and electrochemical reactions in the hybrid system take place at the equilibrium temperature [12].
- 4) All the reactors and heat exchangers are completely insulated. No heat transfer appears between these apparatus and environment.

2.3. Reforming and WGS reactions

The reforming reactions occurring in the SOFC can be described in the following Eqs (1) and (2), which represent methane reforming and WGS reactions, respectively.



In the SOFC, the methane reforming reaction and WGS reaction reach equilibrium in a fast rate due to the high reaction temperature. The components and their concentrations of the product gas mixture after the reforming reaction are closely associated with the equilibrium constant K of the reaction which only depends on the reaction temperature as shown in Eq (3) [13,14].

$$K_{\text{reform}} = \frac{P_{CO} \cdot P_{H_2}^3}{P_{CH_4} \cdot P_{H_2O}} = f(T_{\text{reform}})$$

$$= -2.63121 \times 10^{-11} \cdot T^4 + 1.24065 \times 10^{-7} \cdot T^3 - 2.25232 \times 10^{-4} \cdot T^2 + 0.195028 \cdot T - 66.1395 \quad \text{for reforming reaction} \quad (3)$$

$$K_{\text{WGS}} = \frac{P_{CO_2} \cdot P_{H_2}}{P_{CO} \cdot P_{H_2O}} = f(T_{\text{WGS}})$$

$$= 5.47301 \times 10^{-12} \cdot T^4 - 2.57479 \times 10^{-8} \cdot T^3 + 4.63742 \times 10^{-5} \cdot T^2 - 0.03915 \cdot T + 13.2097 \quad \text{for WGS reaction}$$

2.4. TSA reaction for H_2 separation and purification

The TSA reaction for H_2 separation and purification based on $LaNi_{4.3}Al_{0.7}$ alloy can be written in Eq. (4). The corresponding desorption reaction equilibrium pressure p_{eq} and reaction kinetics are described in Eqs. (5) and (6). The main parameters listed in the equations are shown in Table 1 [15].



$$p_{\text{eq}} = \sum_{n=0}^9 \left[a_n \cdot \left(\frac{H}{M} \right)^n \right] \cdot \exp \left[\frac{\Delta H_{\text{TSA}}}{R_g} \cdot \left(\frac{1}{T_{\text{TSA}}} - \frac{1}{T_{\text{ref}}} \right) \right] \quad (5)$$

$$\dot{m}_{\text{TSA}} = C_a \cdot \exp \left(-\frac{E_{\text{act}}}{R_g T_{\text{TSA}}} \right) \cdot \left(\frac{p_g - p_{\text{eq}}}{p_{\text{eq}}} \right) \cdot (\rho_s - \rho_{\text{HSA}}) \quad (6)$$

Table 1. The main parameters for the TSA reaction based on $\text{LaNi}_{4.3}\text{Al}_{0.7}$ alloy [15].

Parameters	Polynomial coefficients	Desorption rate constant, C_a (s^{-1})	Activation energy, E_{act} (J mol^{-1})	Gas pressure, p_g (bar)	Reaction enthalpy, ΔH_{TSA} (J mol^{-1})
Absorption	$a_0=0.0075, a_1=15.2935, a_2=-34.577,$ $a_3=39.9926, a_4=-26.7998, a_5=11.0397, a_6=-$ $2.8416, a_7=0.446, a_8=-0.0391, a_9=0.0014$ $a_{10}=-1.465, a_{11}=19.190, a_{12}=-42.086,$	59.19	21179.6	1	30100
Desorption	$a_3=49.087, a_4=-33.819, a_5=-14.437, a_6=-$ $3.858, a_7=0.627, a_8=-0.0567, a_9=0.0021$	9.57	23879.6	0.085	

2.5. Fuel cells model

The electrochemical reaction occurring in the fuel cell is written in Eq. (7). The H_2 consumption is determined by the fuel utilization μ_{fuel} of the fuel cells, which is described in Eq. (8).



$$\mu_{\text{fuel}} = \frac{\dot{m}_{\text{H}_2, \text{consumption}}}{\dot{m}_{\text{H}_2, \text{in}}} \quad (8)$$

Equation (9) describes the electrochemical model of fuel cell that the cell voltage V_{cell} equals to the reversible voltage E_N subtracting the irreversible overvoltage V_{act} , V_{ohm} and V_{conc} . The reversible voltages of the SOFC and PEMFC are calculated by Eqs. (10) and (11) [16].

$$V_{\text{cell}} = E_N - V_{\text{act}} - V_{\text{ohm}} - V_{\text{conc}} \quad (9)$$

$$E_{N, \text{SOFC}} = 1.253 - 2.4516 \times 10^{-4} \cdot T_{\text{SOFC}} - \frac{R \cdot T_{\text{SOFC}}}{4F} \cdot \ln \left(\frac{p_{\text{H}_2\text{O}}^2}{p_{\text{H}_2}^2 \cdot p_{\text{O}_2}} \right) \quad (10)$$

$$E_{N, \text{PEM}} = 1.229 - 0.85 \times 10^{-3} \cdot (T_{\text{PEM}} - 298.15) + \frac{R \cdot T_{\text{PEM}}}{4F} \cdot \ln (p_{\text{H}_2}^2 \cdot p_{\text{O}_2}) \quad (11)$$

The activation, ohmic and concentration overvoltage contribute to the irreversible overvoltage. The activation overvoltage V_{act} is caused by the necessary activation of charge transfer for electrodes, which is determined from the Butler-Volmer equation. The activation overvoltage of the SOFC is given by Eq. (12). The exchange current density J_0 in the Eq (12) is related to the electrode microstructure and the operating conditions, which can be written in Eqs (13) and (14). For the PEMFC, the activation overvoltage can be simplified into an empirical equation (15) [17].

$$V_{\text{act, SOFC}} = V_{\text{act, SOFC, a}} + V_{\text{act, SOFC, c}} \quad (12)$$

$$= \frac{R \cdot T_{\text{SOFC}}}{F} \cdot \ln \left[\frac{J}{2J_{0, a}} + \sqrt{\left(\frac{J}{2J_{0, a}} \right)^2 + 1} \right] + \frac{R \cdot T_{\text{SOFC}}}{F} \cdot \ln \left[\frac{J}{2J_{0, c}} + \sqrt{\left(\frac{J}{2J_{0, c}} \right)^2 + 1} \right]$$

$$J_{0, a} = 1.3448 \times 10^{10} \cdot \left(\frac{p_{\text{H}_2}}{p_{\text{ref}}} \right) \cdot \left(\frac{p_{\text{H}_2\text{O}}}{p_{\text{ref}}} \right) \cdot e^{-\frac{E_{\text{act, a}}}{R \cdot T_{\text{SOFC}}}} \quad (13)$$

$$J_{0, c} = 2.051 \times 10^9 \cdot \left(\frac{p_{\text{O}_2}}{p_{\text{ref}}} \right)^{0.25} \cdot e^{-\frac{E_{\text{act, c}}}{R \cdot T_{\text{SOFC}}}} \quad (14)$$

$$V_{act,PEM} = 0.948 - (0.00286 + 0.0002 \ln A + 4.3 \times 10^{-5} \cdot \ln \frac{P_{H_2}}{1.09 \times 10^6 \cdot e^{\frac{77}{T_{PEM}}}}) \cdot T_{PEM} - 7.6 \times 10^{-5} \cdot T_{PEM} \cdot \ln \frac{P_{O_2}}{5.08 \times 10^6 \cdot e^{\frac{498}{T_{PEM}}}} + 1.93 \times 10^{-4} \cdot T_{PEM} \cdot \ln I_{PEM} \tag{15}$$

The ohmic overvoltage $V_{ohm} = I \cdot R_{ohm}$ is caused by the ohmic resistance R_{ohm} of the fuel cell. Generally, the resistance to the protons transfer through the electrolyte mainly contributes to the ohmic resistance in the fuel cell. Therefore, the ohmic overvoltage of the SOFC and PEMFC can be simplified as follows [17,18].

$$V_{ohm} = 2.99 \times 10^{-11} \cdot J \cdot l_e \cdot e^{\frac{10300}{T_{SOFC}}} \quad \text{for the SOFC}$$

$$V_{ohm} = I \cdot \left\{ \frac{181.6 \cdot \left[1 + 0.03 \cdot J + 0.062 \cdot \left(\frac{T_{PEM}}{303} \right)^2 \cdot J^{2.5} \right]}{\left(\psi - 0.634 - 3 \cdot J \cdot e^{\frac{4.18 \cdot T_{PEM} - 303}{T_{PEM}}} \right)} \cdot \frac{l_e}{A} + 0.0003 \right\} \quad \text{for the PEMFC} \tag{16}$$

The concentration overvoltage V_{conc} of the SOFC and the PEMFC are given in Eqs. (17) and (18), respectively [17,19].

$$V_{conc,SOFC} = V_{conc,SOFC,a} + V_{conc,SOFC,c}$$

$$= \frac{R \cdot T_{SOFC}}{2F} \cdot \ln \left(\frac{1 + \frac{R \cdot T_{SOFC} \cdot l_a \cdot J}{2F \cdot D_a^{eff} \cdot P_{H_2O}}}{1 - \frac{R \cdot T_{SOFC} \cdot l_a \cdot J}{2F \cdot D_a^{eff} \cdot P_{H_2}}} \right) + \frac{R \cdot T_{SOFC}}{4F} \cdot \ln \left(\frac{P_{O_2}}{\frac{P_c}{\delta_{O_2}} - \left(\frac{P_c}{\delta_{O_2}} - P_{O_2} \right) \cdot e^{\frac{R \cdot T_{SOFC} \cdot l_c \cdot J \cdot \delta_{O_2}}{4F \cdot D_c^{eff} \cdot P_c}}} \right) \tag{17}$$

$$V_{conc,PEM} = -B \cdot \ln \left(1 - \frac{J}{J_{max}} \right) \tag{18}$$

where, $D_{a/c}^{eff}$ represents the effective diffusion coefficient of the gas through the electrode, which is $D_a^{eff} = \frac{\varepsilon}{\zeta} \cdot \frac{D_{H_2-H_2O} \cdot D_{H_2,k}}{D_{H_2-H_2O} + D_{H_2,k}}$ for the anode and $D_c^{eff} = \frac{\varepsilon}{\zeta} \cdot \frac{D_{O_2-N_2} \cdot D_{O_2,k}}{D_{O_2-N_2} + D_{O_2,k}}$ for the cathode. δ_{O_2} equals to $\frac{\frac{\varepsilon}{\zeta} \cdot D_{O_2,k}}{D_c^{eff} + \frac{\varepsilon}{\zeta} \cdot D_{O_2,k}}$.

The output power of the fuel cell stack is given by the following equation:

$$P_{FC} = N \cdot J \cdot A \cdot V_{cell} \tag{19}$$

3. Results and discussion

3.1. Model validation

This simulation in this work is carried out by the software MATLAB/SIMULINK with the relative tolerance of 0.001. The validation of the SOFC model is performed using the experimental data in Ref [20]. The corresponding operating and geometrical parameters in experiment are summarized in Table 2. Fig. 2a shows the comparison between the simulation results and the experimental data at different temperatures. It can be clearly seen that a good agreement appears between the simulation and the experiment, strongly indicating that the SOFC model in this paper can be used to accurately predict the SOFC performance. Similarly, Fig. 2b also proves the good agreement between the simulation results and the experimental data [21] when using the PEMFC model to predict the performance at 343 K. The relevant operating and geometrical parameters in experiment are also summarized in Table 2.

Table 2. The main parameters for the model validation [20-23].

	Parameters	Values
SOFC	H ₂ pressure at the anode electrode p_{H_2} , bar	0.97
	H ₂ O pressure at the anode electrode p_{H_2O} , bar	0.03

	O ₂ pressure at the cathode electrode p_{O_2} , bar	0.21
	Operating cathode pressure p_c , bar	1
	Anode thickness l_a , m	0.001
	Electrolyte thickness l_e , m	8×10^{-6}
	Cathode thickness l_c , m	20×10^{-6}
	Electrode porosity ε	0.48
	Electrode tortuosity ζ	5.4
	H ₂ pressure at the anode electrode p_{H_2} , bar	1
	O ₂ pressure at the cathode electrode p_{O_2} , bar	1
	Cell active area A , cm ²	50.6
PEMFC	Electrolyte thickness l_e , cm	0.0178
	Coefficient ψ	23
	Coefficient B	0.016
	Maximum current density J_{\max} , A m ⁻²	1.5

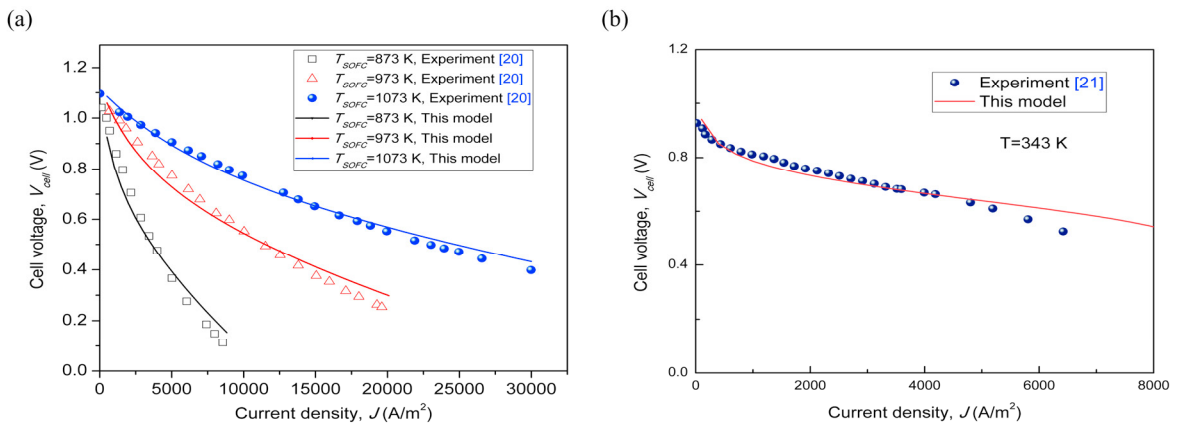


Fig. 2. The model validation, (a) SOFC, (b) PEMFC.

3.2. System performance

Based on the established model, the performance of the NG-fueled SOFC-PEMFC hybrid system coupled with the TSA treatment is first investigated under the fixed operating conditions of NG mass flow $\varphi_{\text{NG}} = 0.5$ mol/s, steam-to-carbon ratio $\tau_{\text{S/C}} = 2.5$, HT-WGS and LT-WGS temperatures $T_{\text{HT-WGS}} = 623$ K and $T_{\text{LT-WGS}} = 473$ K. Fig. 3a displays the output characteristics of the SOFC-PEMFC hybrid system with the variation of the SOFC fuel utilization when the operating temperatures of the SOFC and PEMFC are 1073 and 343 K, respectively. Here, it is noteworthy that the hydrogen desorption reaction temperature occurring in the TSA reactor determines the PEMFC operating temperature. Besides, the TSA equilibrium pressure is the input H₂ pressure for the PEMFC. That is to say, the PEMFC operating conditions could be adjusted through controlling the TSA process.

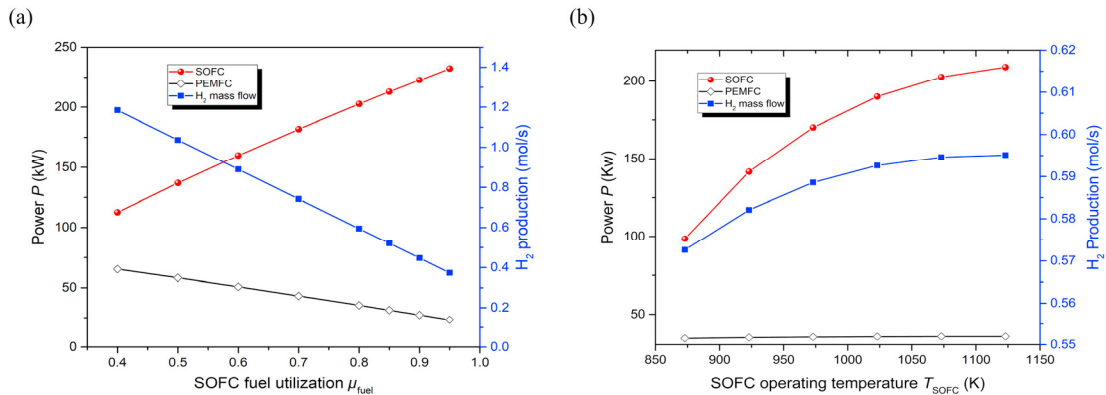


Fig. 3. The performances of the hybrid system at different conditions, (a) variation with the SOFC fuel utilization, (b) variation with the SOFC operating temperature.

It can be clearly seen from Fig. 3a that the output power of the SOFC increases as more fuel is utilized in the SOFC. However, the H₂ production is reduced because of more H₂ consumed for SOFC power generation. As a result, the power generation of the PEMFC depending on the H₂ fuel is also reduced from 65.32 to 23.27 kW when the μ_{fuel} is increased from 0.4 to 0.95. Since the μ_{fuel} has a bigger influence on the SOFC than the PEMFC, the total output power of the hybrid system increases with the increase of μ_{fuel} . The energy conversion efficiency of the hybrid system coupled with the TSA is calculated to be approximately 64%, which is much higher than the only-SOFC (about 43%) and the reform-PEMFC (about 40%) systems [24,25]. Fig. 3b shows the influences of the SOFC operating temperature on the hybrid system when the μ_{fuel} and the T_{PEMFC} are set to be 0.8 and 343 K, respectively. The T_{SOFC} has a significant influence on the output power of the SOFC but a slight influence on the H₂ production and PEMFC output.

3.3. Dynamic responses

The dynamic response behaviors of the SOFC-PEMFC hybrid system coupled with the TSA process are further investigated. Compared to the electrical response, the response to the fuel input rate is much slower for the fuel cells system, indicating that the fuel rate response dominates the FC dynamic behaviors. The time constant τ of the fuel input rate is about the order of magnitude of ~ 1 s [26]. We choose $\tau=5$ s as the time constant of the fuel rate in this work. Therefore, the fuel NG input into the SOFC changes with the time in the function of $\varphi_{NG} = 0.5 \cdot \left(1 - e^{-\frac{t}{\tau}}\right)$.

The dynamic response behaviors of the hybrid system are predicted under the NG loading variation. The operating conditions of the fuel cells are set as $\mu_{fuel} = 0.8$, $T_{SOFC} = 1073$ K and $T_{PEMFC} = 343$ K.

Figure 4 shows the dynamic response behaviors of the hybrid system to the NG fuel varying in the function $\varphi_{NG} = 0.5 \cdot \left(1 - e^{-\frac{t}{\tau}}\right)$. It can be seen that the SOFC and PEMFC present different dynamic characteristics to the fuel rate.

The SOFC needs approximately 15 s to reach stable power output ($P_{SOFC}=248$ kW), while it takes about 10 s for the PEMFC achieving the steady-state with $P_{PEMFC}=26$ kW. The comparison suggests that the PEMFC response time to the varying NG input is smaller than the SOFC response time. However, the SOFC output power is much larger, which is about 9 times as large as the PEMFC power. Therefore, the SOFC power mainly contributes to the hybrid system power generation. Considering the transient behavior of the hybrid system, the PEMFC plays a more important role than the SOFC. In conclusion, the power distribution between SOFC and PEMFC in the hybrid system is significant to balance the power capacity and transient behavior. The further discussions and analyses about the FC power distribution strategy are also in preparation.

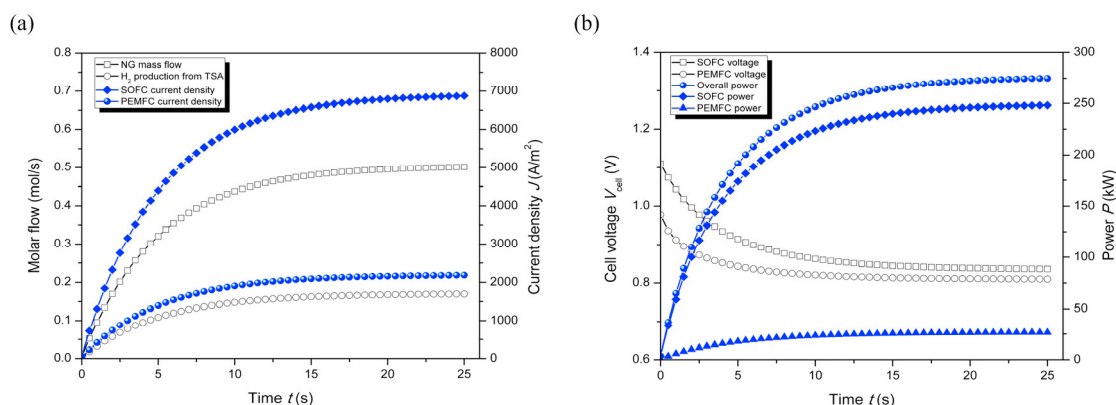


Fig. 4. The dynamic responses of the hybrid system to the NG input varying load, (a) H_2 production from the TSA and the current density, (b) cell voltage and power.

4. Conclusions

The SOFC-PEMFC hybrid system coupled with the TSA process for H_2 separation and purification is proposed and modeled in this work. The hybrid power system presents a much higher energy conversion efficiency than the standalone SOFC or the reformer-PEMFC power system. In the hybrid system, the SOFC contributes to most of the power generation, while the PEMFC dominates the transient response. The operation strategy should be further determined to optimize the performance of the hybrid system.

Acknowledgements

This work is partially supported by the Hong Kong Scholar Program (No. XJ2017023), the National Natural Science Foundation of China (No. 51506174) and the Natural Science Foundation of Shaanxi Province (No. 2017JQ5059).

References

- [1] Yeager E. Fuel cells. *Science* 1961; 134: 1178-1186.
- [2] Xu HR, Chen B, Tan P, Cai WZ, He W, Farrusseng D, Ni M. Modeling of all porous solid oxide fuel cells. *Appl Energy* 2018; 219: 105-113.
- [3] Liu YF, Fan L, Pei PC, Yao SZ, Wang F. Asymptotic analysis for the inlet relative humidity effects on the performance of proton exchange membrane fuel cell. *Appl Energy* 2018; 213: 573-584.
- [4] Dicks AL, Fellows RG, Mescal CM, Seymour C. A study of SOFC-PEM hybrid systems. *J Power Sources* 2000; 86: 501-506.
- [5] Rabbani A, Rokni M. Modeling and analysis of transport processes and efficiency of combined SOFC and PEMFC systems. *Energies* 2014; 7: 5502-5522.
- [6] Lulianelli A, Ribeirinha P, Mendes A, Basile A. Methanol steam reforming for hydrogen generation via conventional and membrane reactors: A review. *Renew Sustain Energy Rev* 2014; 29: 355-368.
- [7] Fernandes A, Woudstra T, van Wijk A, Verhoef L, Aravind PV. Fuel cell electric vehicle as a power plant and SOFC as a natural gas reformer. An exergy analysis of different system designs. *Appl Energy* 2016; 173: 13-28.
- [8] Moen OM, Stene HS. Power plant with CO_2 capture based on PSA cycle. Master Thesis, Norwegian University of Science and Technology, Trondheim, Norway, 2014.
- [9] Wang QD, Wu J, Chen CP, Luo WF, Fang TS. Study on the hydrogen purification technology and apparatus based on metal hydride. *Sci Technol Bull Chin* 1985; 1: 1-3.
- [10] Yang FS, Chen XY, Wu Z, Wang SM, Wang GX, Zhang ZX, Wang YQ. Experimental studies on the poisoning properties of a low-plateau hydrogen storage alloy $LaNi_{4.3}Al_{0.7}$ against CO impurities. *Int J Hydrogen Energy* 2017;42: 16225-16234.
- [11] Stiller C, Thorud B, Seljebø S, Mathisen Ø, Karoliussen H, Bolland O. Finite-volume modeling and hybrid-cycle performance of planar and tubular solid oxide fuel cells. *J Power Sources* 2005; 141: 227-240.
- [12] Aguiar P, Adjiman CS, Brandon NP. Anode-supported intermediate temperature direct internal reforming solid oxide fuel cell. I: model-based steady-state performance. *J Power Sources* 2004; 138: 120-136.
- [13] Calise F, d'Accadia MD, Palombo A, Vanoli L. Simulation and exergy analysis of a hybrid solid oxide fuel cell (SOFC)-gas turbine system. *Energy* 2006;31: 3278-3299.

- [14] Parmar RD, Kundu A, Thrugood C, Peppley BA, Karan K. Kinetic studies of the autothermal reforming of tetradecane over Pt/Al₂O₃ catalyst in a fixed-bed reactor. *Fuel* 2010; 89: 1212-1220.
- [15] Jemni A, Nasrallah SB, Lamoumi J. Experimental and theoretical study of a metal-hydrogen reactor. *Int J Hydrogen Energy* 1999; 24: 631-644.
- [16] Cheddie DF. Integration of a solid oxide fuel cell into a 10 MW gas turbine power plant. *Energies* 2010; 3: 754-769.
- [17] Correa JM, Farret FA, Canha LN, Simoes MG. An electrochemical-based fuel-cell model suitable for electrical engineering automation approach. *IEEE T IND ELECTRON* 2004; 51: 1103-1112.
- [18] Ferguson JR, Fiard JM, Herbin R. Three-dimensional numerical simulation for various geometries of solid oxide fuel cells. *J Power Sources* 1996; 58: 109-122.
- [19] Ni M, Leung M, Leung D. Parametric study of solid oxide fuel cell performance. *Energy Convers Manage* 2007; 48: 1525-1535.
- [20] Zhao F, Virkar AV. Dependence of polarization in anode-supported solid oxide fuel cells on various cell parameters. *J Power Sources* 2005; 141: 79-95.
- [21] Ceraolo M, Miulli C, Pozio A. Modelling static and dynamic behavior of proton exchange membrane fuel cells on the basis of electrochemical description. *J Power Sources* 2003; 113: 131-144.
- [22] Chan SH, Khor KA, Xia ZT. A complete polarization model of a solid oxide fuel cell and its sensitivity to the change of component thickness. *J Power Sources* 2001; 93: 130-140.
- [23] Yakabe H, Hishinuma M, Uratani M, Matsuzaki Y, Yasuda I. Evaluation and modeling of performance of anode-supported solid oxide fuel cell. *J Power Sources* 2000; 86: 423-431.
- [24] Riensche E, Stimming U, Unverzagt G. Optimization of a 200 kW SOFC cogeneration power plant Part I : Variation of process parameters. *J Power Sources* 1998;73: 251–256.
- [25] Marcoberardino GD, Roses L, Manzolini G. Technical assessment of a micro-cogeneration system based on polymer electrolyte membrane fuel cell and fluidized bed autothermal reformer. *Appl Energy* 2016;162: 231–244.
- [26] Dick AL, Martin PA. A fuel cell balance of plant test facility. *J Power Sources* 1998;71: 321–327.